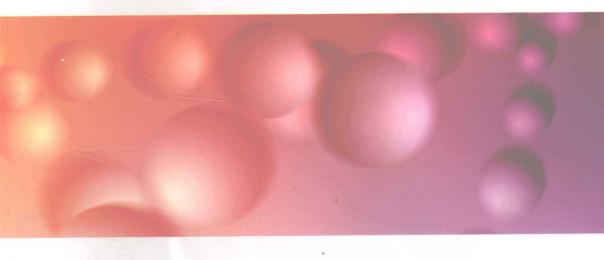
System Design and Application of Magnetostrictive Biosensor

(磁致伸缩生物传感器系统设计和应用)

Zhang Kewei Zhang Shaoqin





System Design and Application of Magnetostrictive Biosensor

(磁致伸缩生物传感器系统设计和应用)

Zhang Kewei Zhang Shaoqin





Responsible Editors: Qian Jun, Liu Xinli

© 2011 Science Press 16 Donghuangchenggen North Str. Beijing, China

All rights are reserved. No part of this book covered by the copyright hereon may be reproduced or used in any form or by any means—graphic, electronic, or mechanical, including photocopying, recording, taping, or information storage and retrieval system—without permission of the publisher.

Published by Science Press Ltd.

ISBN: 978-7-03-032532-7

Preface

Food-borne disease caused by pathogenic bacteria is a major concern all over the world, and it attracts a great of attention of people and the governments, relevant international organizations and academic institutions. Therefore, there is an urgent need for detection technologies that can rapidly detect/monitor the presence of pathogens in food. Various detection technologies have been recently developed and investigated. Among these technologies, biosensor technologies provide many unique advantages over others.

In this book, the knowledge about magnetostrictive biosensor system design and applications of magnetostrictive biosensors for bacterial detection were introduced.

Chapter 1 introduced the background of food safety and security, the basic knowledge about pathogenic bacteria and food-borne illness and also the knowledge about conventional bacterial detection methods and advanced biosensor techniques. Regarding biosensors, electrochemical biosensors, acoustic wave (AW) biosensors and micro-cantilever (MC) based biosensors were discussed. In addition, recently developed magnetostrictive micro-cantilever (MSMC)-based biosensors and magnetostrictive particle (MSP) based biosensors were also introduced.

Chapter 2 introduced the resonance behavior and influence of surrounding media on the resonance behavior of MSP based sensors. The resonance behavior of MSP sensors in viscous media is unveiled. In this chapter, both resonance frequency and Q value of MSP based sensors in different sizes/dimensions and in different media were investigated.

Chapter 3 introduced the techniques in design and fabrication of phage/antibody immobilized magnetostrictive biosensor for bacterial detection. Using an MSP as a sensor platform, an MSP based biosensor has many unique advantages, such as wireless, high sensitivity, easy operation, and working well in liquid. In this chapter, phage immobilized MSP biosensors for the detection of *S. typhimurium* and antibody-immobilized MSP biosensors for the detection of *E. coli* and *L. Monocytogenes* are fully presented.

Chapter 4 introduced the design and simulating technique for advanced portable MSP biosensor system. Two different techniques are introduced: one is based on

frequency-domain technique, and the other one is based on time-domain technique. A special simulating technique based on the equivalent circuit using MATLAB to analyse the resonance behavior (i.e. phase and gain) is introduced. The application of the two techniques for bacterial detection was also presented in this chapter.

One of the final goals of MSP based biosensors is to be able to detect a target with extremely small mass such as virus. In this case, the sensor size has to be decreased down to nano-scale. However, it is difficult to decrease the size of currently commercial available magnetostirctive material down to nano-scale. In Chapter 5, a template based electro-chemical deposition method was introduced for the synthesis of amorphous magnetostrictive nanowires to obtain a highly sensitive biosensor platform.

Chapter 6 introduced the future perspectives of magnetostrictive biosensor system and also gave some suggestions to further improve the performance of magnetostrictive biosensor system.

The authors would like to express our appreciation to the Shanxi Province Government, Taiyuan University of Science and Technology, Auburn University and Professors Z. Y. Cheng, Bryan A. Chin and other colleges acknowledged in Dr. Kewei Zhang's doctoral dissertation.

List of Abbreviations

FDA Food and drug administration

CDC Centers for disease control and prevention

ELISA Enzyme-linked immunosorbent assay

PCR Polymerase chain reaction

DNA Deoxyribonucleic acid

SPR Surface plasmon resonance

ISE Ion-selective electrode

ISFET Ion-sensitive field effect transistors

AW Acoustic wave

QCM Quartz crystal microbalance

TSM Thickness shear microbalance

SAW Surface acoustic wave

IDT Interdigital transducer

APM Acoustic wave plate mode

SH-APM Shear-horizontal acoustic wave plate mode

FPW Flexural plate wave

MC Micro-cantilever

MSMC Magnetostrictive micro-cantilever

AC Alternating current

DC Direct current

PAbs Polycolonal antibodies

MAbs Monoclonal antibodies

MSP Magnetostrictive particles NSB Non-specific binding

BSA Bovine serum albumin

BOVINE SETUIN AIDUMINI

PBS Phosphate buffered saline
TBS Tris buffered saline

PC Personal computer

SEM Scanning electron microscopy

EDTA Ethylenediaminetetraacetic acid

• xviii • System Design and Application of Magnetostrictive Biosensor

DUT Device under test
GUI Graphical user interface
FCC Face centered cubic

List of Symbols

$S_{ m m}$	Mass sensitivity
Q	Quality merit factor
f_n	n th harmonic resonance frequency
L	Length
W	Width
ν	Acoustic velocity
E	Young's modulus
ρ	Density
υ	Poisson ratio
m	Power value
$U^{\!\star}(\omega)$	Potential through DUT
${U_{\rm r}}^*(\omega)$	Potential through a reference
$Z^{*}(\omega)$	Impedance of DUT
$Z_{\rm r}^*(\omega)$	Impedance of a reference
F	Faraday
H	Henry
Ω	Ohm
$f_{ m r}$	Resonance frequency
$f_{ m ar}$	Anti-resonance frequency

Contents

Preface1			
List of figuresvii			
Li	st of ta	bles	xv
Li	st of al	bbrevi	iationsxvii
Li	st of sy	mbol	s xix
1	Intro	ductio	on
	1.1	Intro	duction to pathogenic bacteria and food-borne illness 1
		1.1.1	Foodborne pathogenic bacteria
		1.1.2	Infectious dose and detection of bacteria4
	1.2	Conv	ventional bacterial detection methods
		1.2.1	Plate counting methods5
		1.2.2	Enzyme-linked immunosorbent assay (ELISA)6
		1.2.3	Polymerase chain reaction (PCR)
	1.3	Bios	ensors9
		1.3.1	Optical biosensors
		1.3.2	Electrochemical biosensors
		1.3.3	Acoustic wave (AW) biosensors14
		1.3.4	Micro-cantilever (MC) based biosensors
		1.3.5	Magnetostrictive micro-cantilever (MSMC)-based biosensors
	1.4	Mag	netostrictive particle (MSP) based biosensors
		1.4.1	Resonance behavior of MSP
		1.4.2	Resonance behavior of MSP in viscous media
		1.4.3	Magnetostrictive effect and materials
		1.4.4	Current status of biosensors based on MSPs
	1.5	Sens	ing element for biosensors—antibodies vs. phages
	1.6	Rese	arch objectives
	Refe	erence	s
2	Reso	nance	behavior of msp and influence of surrounding media 37
	2.1	Intro	duction
	2.2	Char	racterization of the resonance behavior of an MSP

		4.3.2 Time-domain technique	106
	4.4	Conclusions	114
	Refe	erences	115
5	Syntl	nesis of amorphous magnetostrictive thin film/nanowires using	
	elect	rochemical deposition method	116
	5.1	Introduction	116
	5.2	Materials preparation	117
	5.3	Electrochemical deposition of amorphous Co-Fe-B thin films	117
	5.4	Electrochemical deposition of Co-Fe-B nanobars/nanotubes	122
	5.5	Results and discussion	124
	5.6	Conclusions	133
	Refe	erences	134
6	Futur	re nerspectives and recommendations	136

List of Figures

Figure 1-1	Schematic of different colony counting techniques where the white dots represent
	the bacteria colonies and the grey circles represent the agar plate6
Figure 1-2	Illustration of enzyme labeled antibody ELISA6
Figure 1-3	An illustration of the polymerase chain reaction (PCR)8
Figure 1-4	Schematic illustration of a typical biosensor system9
Figure 1-5	A typical prism-based surface plasmon resonance biosensor configuration11
Figure 1-6	Scheme of frequency vs. signal amplitude of an AW sensor, where f_0 and $f_{ m mass}$ are the
	resonance frequency of the sensor without mass load and with mass load, respectively 14
Figure 1-7	Schematic definition of Q value. The resonance peak is at frequency f_0 with a height
	of h
Figure 1-8	Schematic illustration of an acoustic plate mode (APM) device16
Figure 1-9	Diagram of Lamb wave modes
Figure 1-10	Illustration of cantilever array readout by optical beam deflection21
Figure 1-11	Illustration of a fluid filled micro-cantilever
Figure 1-12	Configuration of a magnetostrictive micro-cantilever
Figure 1-13	Schematic of working principle of a magnetostrictive biosensor
Figure 1-14	(a) Smooth surface; (b) rough surface with trapped liquid particles; (c) equivalent attached
	liquid layer on the smooth surface. The solid circles represent liquid particles. R denotes the
	variation of the mountains and valleys where the mountains and valleys were assumed to be
	evenly and uniformly distributed on the MSP surface. $R_{\rm ave}$ denotes the average surface
	roughness (i.e. average thickness of the trapped liquid layer)
Figure 1-15	Magnetostriction response of a magnetostrictive material: mechanical strain (λ)
	in relation to external magnetic field (H)
Figure 1-16	Schematic structure of a filamentous phage
Figure 1-17	Configuration of a typical antibody structure
Figure 2-1	Configuration of a network analyzer with an S-parameter test set
Figure 2-2	A typical magnitude and phase curve of S_{11} parameter changing with the frequency
	of an MSP
Figure 2-3	Resonance frequency (f_1) of the 1 st harmonic mode $(n = 1)$ of MSPs41
Figure 2-4	$2Lf_1$ in relation to L for the MSPs with different L/W ratios

Figure 2-5	The Q value of MSPs with different sizes and geometries
Figure 2-6	The length dependence of the resonance frequency $(f_{1,i})$ of first harmonic mode for
	MSPs in different liquids
Figure 2-7	The " $2 \cdot L \cdot f_{1,l}$ " in relation to the L for the MSPs with different L/W ratios, where the $f_{1,l}$
	is the resonance frequency of the first harmonic mode of MSPs in liquids4
Figure 2-8	The " $2 \cdot L \cdot f_{1,l}$ " in relation to the L/W ratio for the MSPs with different lengths, where
	the $f_{1,l}$ is the resonance frequency of the first harmonic mode of MSPs in liquids4
Figure 2-9	$\Delta f_n/\rho_l$ vs. $\sqrt{\eta/\rho_l}$ for two similar MSPs in different liquids4
Figure 2-10	$\Delta f_n/\rho_l$ vs. $\sqrt{\eta/\rho_l}$ for two similar MSPs in different liquids4
Figure 2-11	$\Delta f_n/\rho_l$ vs. $\sqrt{\eta/\rho_l}$ for MSPs with the same width but different lengths in different
	liquids, where the MSPs were operated at first harmonic mode4
Figure 2-12	Δf_n in relation to $(f_n)^{0.5}$ for an MSP in different media. The size of the MSP is
	15.52 mm \times 3.78 mm \times 30 μ m and three harmonic modes (1st, 3rd, 5th) are
	presented5
Figure 2-13	The $1/Q$ vs. $\sqrt{\rho_l \eta}$ for two similar sizes of MSPs (MSP-1: 15.52 mm × 3.78 mm × 30 μ m
	and MSP-2: 15.58 mm \times 3.76 mm \times 30 $\mu m) in different liquids$
Figure 2-14	$\Delta f_n/\rho_l$ vs. $\sqrt{\eta/\rho_l}$ for MSPs with the same width but different lengths in different
	liquids, where the MSPs were operated at first harmonic mode5
Figure 3-1	Schematic illustration of modification of antibodies (top) and the immobilization
	of the modified antibody onto gold coated MSP (bottom)5
Figure 3-2	Schematic configuration of the experimental setup for the characterization
	of the response of MSP biosensor in liquid analyte6
Figure 3-3	Scheme of (a) the sequences of the analytes through the test chamber (tube); (b) the
	typical sensor response 6
Figure 3-4	(a) Stable/saturated shift in the resonance frequency shift of an MSP sensor in
	relation to the population of the analyte. (b) A typical Hill plot obtained from
	the data shown in Figure (a)6
Figure 3-5	A typical dynamic dose response of a phage E2 immobilized magnetostrictive
	biosensor in the size of 1.0 mm \times 0.3 mm \times 15 μm to increasing population of
	S. typhimurium
Figure 3-6	Resonance frequency shifts (Hz) change with the increasing population of
	the S. typhimurium6
Figure 3-7	Hill plot from the dose response curve6
Figure 3-8	The dynamic dose response of an antibody immobilized sensor to the increasing
	population of E. coli

Figure 3-9	Resonance frequency shifts (Hz) change with the increasing population of the E. coli
	suspensions (cfu/ml)
Figure 3-10	Hill plot from the dose response curve
Figure 3-11	The dynamic dose response of an antibody immobilized sensor to the increasing
	population of S. aureus69
Figure 3-12	Resonance frequency shift (Hz) of the sensors with different treatment70
Figure 3-13	Hill plot from the dose response curve
Figure 3-14	A dynamic dose response of an antibody immobilized magnetostrictive sensor to
	increase populations
Figure 3-15	Resonance frequency shift (Hz) of the sensors with different treatment: the
	antibody immobilized sensor (square) and a reference sensor (dot) change with the
	increasing population of the <i>L. monocytogene</i> suspensions
Figure 3-16	The Resonance frequency shift (Hz) of the sensors with different treatment:
	magnetostrictive biosensors (square), reference sensors (dot), casein blocked controlled
	sensors (triangle), and BSA blocked controlled sensors (reciprocal triangle)72
Figure 3-17	Hill plot from the dose response curve showing the kinetics of antibody and bacteria
	binding
Figure 3-18	SEM images of L. monocetogenes on (a) the casein controlled sensor; (b) the
	BSA controlled sensor; (c) the reference sensor (devoid of antibody immobilization),
	and (d) the antibody-immobilized magnetostrictive sensor
Figure 4-1	The equivalent circuit of the device under test (DUT). (a) The overall equivalent
	circuit. (b), (c), and (d) show the details of the equivalent circuit for three main
	parts of the circuit shown in (a), where R , L and C are resistor, inductor, and capacitor,
	respectively
Figure 4-2	Frequency dependence of the impedance $Z(\omega)$ of a magnetic resonator in a coil78
Figure 4-3	Schematic of time domain technique, (a) a pulse current is applied on to a DUT;
	(b) a voltage across the two ends of the DUT is generated. The voltage changes
	with the time
Figure 4-4	The schematic circuit for (a) the DUT; (b) the reference
Figure 4-5	Fitting for the resonance phase behavior of a sensor in the size of 1.0 mm \times 0.3 mm \times 30 μm
	in air. The dash lines are the fitting results while the solid lines are the experimental
	results82
Figure 4-6	(Left) block diagram of the interrogation device, (right) picture of the interrogation
	device
Figure 4-7	The picture of the circuit built based on the design shown in Figure 4-583

Figure 4-8	The holder built on a circuit board, where both reference and DUT channels are
	included. The backside of the board is grounded84
Figure 4-9	The graphical user interface (GUI)85
Figure 4-10	Resonance spectrum of the sensor using different device: (a) phase in relation to
	frequency; (b) amplitude and gain in relation to frequency where the solid line
	represents the measured result using network analyzer and the dash line represents
	the measured result using the indirect approach86
Figure 4-11	(a) Phase of $Z(\omega)$ frequency in air in relation to frequency in water; (b) gain of $Z(\omega)$
	in relation to frequency in air and in water87
Figure 4-12	Phase signal of MSP in coil in relation to frequency. (a) MSP in size of
	$0.75~mm \times 0.15~mm \times 30~\mu m;$ (b) MSP in size of 0.5 mm \times 0.1 mm \times 30 $\mu m.$
	The dash lines are the results for MSPs in water, while the solid lines are the
	results for MSPs in air
Figure 4-13	Schematic configuration of a capacitor in parallel with the DUT89
Figure 4-14(a)	The phase in relation to frequency for an MSP in a coil. The different curves are
	the results of different capacitors in parallel with the DUT. The capacitance
	(C _x) of each capacitor is given in this figure89
Figure 4-14(b)	The gain in relation to frequency for an MSP in a coil. The different curves are
	the results of different capacitors in parallel with the DUT. The capacitance (C_x)
	of each capacitor is given in this figure90
Figure 4-15	(a) Phase in relation to frequency; (b) absolute value of phase in relation to
	frequency. In (a) from top to bottom, the curves correspond the increase in the
	capacitance of C_x
Figure 4-16	The phase peak amplitude in relation to capacitance of C_x 92
Figure 4-17	Schematic configuration of a capacitor in series with the DUT93
Figure 4-18(a)	The phase in relation to frequency for an MSP in a coil. The different curves
	are the results with different capacitors in series with the DUT. The capacitance
	of each capacitor is given in this figure
Figure 4-18(b)	The gain in relation to frequency for an MSP in a coil. The different curves
	are the results with different capacitors in series with the DUT. The capacitance
	of each capacitor is given in this figure
Figure 4-19	The simulation of phase in relation to frequency. The curves from top to bottom
	correspond to the increase in the capacitance of C_x
Figure 4-20	Phase peak amplitude in relation to capacitance of C_x
Figure 4-21	Schematic configuration of a resistor in parallel with the DUT95

Figure 4-22(a)	The phase in relation to frequency for an MSP in a coil. The different curves	
	are the results of different resistors in parallel with the DUT. The resistance	
	of each resistor is given in this figure	.96
Figure 4-22(b)	The gain in relation to frequency for an MSP in a coil. The different curves	
al al	are the results of different resistors in parallel with the DUT. The resistance	
	of each resistor is given in this figure	.96
Figure 4-23	The simulation of phase in relation to frequency. The curve moves from bottom to	
	top corresponding to the increase in the resistance of R_x	.97
Figure 4-24	Phase peak amplitude in relation to resistances of R _x	.98
Figure 4-25	Schematic configuration of a resistor in series with the DUT	.98
Figure 4-26(a)	The phase in relation to frequency for an MSP in a coil. The different curves are	
	the result of different resistors in series with the DUT. The resistance of each resistor	
	is given in this figure	.99
Figure 4-26(b)	The gain in relation to frequency for an MSP in a coil. The different curves	
	are the result of different resistors in series with the DUT. The resistance of	
	each resistor is given in this figure	.99
Figure 4-27	The phase in relation to frequency for an MSP in a coil. The curves from the top to	
	the bottom correspond to the increase in the resistance of R_x	100
Figure 4-28	Phase peak amplitude in relation to resistances of R _x	100
Figure 4-29	New design for DC and AC coils	101
Figure 4-30	Phase in relation to frequency under different DC current	102
Figure 4-31	(a) Resonance frequency in relation to DC for the same sensor; (b) phase peak	
	amplitude in relation to DC for the same sensor.	102
Figure 4-32	Schematic configuration I of the holder where two sensors (MSP-1 and MSP-2)	
	were put in one coil	103
Figure 4-33	The phase signal vs. frequency for two sensors (MSP-1 and MSP-2) in one coil	103
Figure 4-34	Schematic configuration II of the holder where two coils are connected in parallel	104
Figure 4-35	The phase signal vs. frequency for two coils: coil-1 and coil-2 connected in paral	lel.
	The MSP-1 was placed in coil-1 and MSP-2 was placed in coil-2	104
Figure 4-36	Schematic configuration III of the holder where two coils were connected in series	105
Figure 4-37	The phase signal vs. frequency for two coils: coil-1 and coil-2 connected in series	s.
¥	The MSP-1 was placed in coil-1 and MSP-2 was placed in coil-2	105
Figure 4-38	Resonance frequency shift (Hz) change with the increasing population of the	
	S. typhimurium suspensions	106
Figure 4-39	Schematic definition of a square pulse as a function of time	107

Figure 4-40	Schematic diagram of an FT magnitude spectrum of a square pulse107
Figure 4-41	(a) Signal amplitude vs. time; (b) signal amplitude vs. frequency108
Figure 4-42	Schematic block diagrams for the time-domain interrogation device
Figure 4-43	(a) Picture of the circuitry based on the design; (b) picture of circuitry in the metal
	box as shown in Figure 4-44(a)109
Figure 4-44	(a) Picture of the holder; (b) schematic diagram of the driving and pick-up coils 109
Figure 4-45	The graphical user interface (GUI)
Figure 4-46	The power spectrum vs. frequency for an MSP sensor111
Figure 4-47	The power spectrum vs. frequency for (a) two sensors (MSP-1 and MSP-2) in air
	and in water; (b) two sensors (MSP-3 and MSP-4) in air and in water112
Figure 4-48	The power spectrum vs. frequency under different pulse voltages for an MSP
	sensor
Figure 4-49	The dose response of a magnetostrictive phage immobilized sensor (square),
	reference sensor (dot), and casein blocked sensor (triangle)114
Figure 5-1	Electrochemical cell for Co-Fe-B thin film deposition
Figure 5-2	XRD patterns of Co-Fe-B thin films with different deposition currents
Figure 5-3	XRD patterns of Co-Fe-B thin films with different amount of DMAB121
Figure 5-4	XRD patterns of Co-Fe-B thin films with different amount of FeSO ₄ 122
Figure 5-5	Template synthesis of Co-Fe-B nanobars/nanotubes
Figure 5-6(a)	Partially gold covered template, deposition current: 15 mA, deposition time:
	1 min, initial concentration
Figure5-6(b)	Partially gold covered template, deposition current: 15 mA, deposition time:
	3 min, initial concentration
Figure5-6(c)	Partially gold covered template, deposition current: 15 mA, deposition time:
	6 min, initial concentration
Figure 5-6(d)	Partially gold covered template, deposition current: 15 mA, deposition time:
	15 min, initial concentration
Figure 5-6(e)	Partially gold covered template, deposition current: 1 mA, deposition time:
	3 min, initial concentration
Figure 5-6(f)	Partially gold covered template, deposition current: 5 mA, deposition time:
	3 min, initial concentration
Figure 5-6(g)	Partially gold covered template, deposition current: 10 mA, deposition time:
	15 min, initial concentration
Figure 5-6(h)	Partially gold covered template, deposition current: 15 mA, deposition time:
	6 min, 1/4 initial concentrations